CrossMark

The Role of Metal Vapour in Gas Metal Arc Welding and Methods of Combined Experimental and Numerical Process Analysis

M. Hertel[1] · M. Trautmann[1] · S. Jäckel[1] · U. Füssel[1]

Abstract Gas metal arc welding (GMAW) processes are characterized by a high number of simultaneously running physical processes. The process capability is mainly determined by the properties of a metal vapour influenced arc and the material transfer. In recent years, experimental as well as numerical methods are being used increasingly in order to understand the complex interactions between the arc and material transfer. In this paper, we discuss the influence of metal vapour on GMAW processes in spray as well as pulsed material transfer mode. With respect to the high complexity of the process, experimental and numerical methods are combined in a targeted manner in order to obtain a high level of expressive capability with moderate numerical and experimental effort. The results illustrate the high influence of the changing vaporization rate not only on the arc properties but on the arc attachment at the filler wire. It could be shown, that in many cases the metal vapour concentration in the arc region has a greater influence on the arc properties and the material transfer than different shielding gas components like oxygen, hydrogen or helium.

Keywords Numerical simulation · Gas metal arc welding (GMAW) · Metal vapour · Material transfer · Droplet detachment

Introduction

Gas metal arc welding (GMAW) is one of the most common welding processes in order to join a wide range of metallic materials. In GMAW an electric arc is established between a continuously fed consumable filler wire and a parent material while the process is protected by a so called shielding gas. Usually, the filler wire has an anodic and the parent material a

✉ M. Hertel
  Martin.Hertel@tu-dresden.de

1 Technische Universität Dresden, Dresden, Germany

🦋 Springer

cathodic polarity. A schematic illustration of the gas metal arc welding process is shown on the left hand side of Fig. 1.

Due to the heating effect of the arc, the electrodes are melted, leading to formation of droplets at the filler wire. These droplets are detached from the filler wire under the influence of gravity force and electromagnetic pinch force. Depending on the characteristic of the power source and the ratio between the feeding rate and the melting rate of the filler wire, different modes of material transfer, like short-circuit, globular or spray-type transfer, accrue. These material transfer modes are numerously described in the literature [1, 2] and are illustrated on the right hand side of Fig. 1.

During the heating of the filler wire, a high amount of metal vapour is generated which is afterwards transported through the centre of the arc. Due to the varying shapes of the filler wire and the metal vaporization there are strong interactions between the arc and the material transfer, which mainly determine the process capabilities of GMAW.

Numerous experimental studies have been carried out to understand the interactions between the arc and the vaporizing filler wire in GMAW. Many of these investigations are summarized by Murphy [2, 3]. Spectroscopic investigations on GMAW arcs [4–8] show that the temperature distribution differs significantly from those of Tungsten Inert Gas (TIG) welding arcs. For arcs in pure argon, the temperature was found to have a local radial minimum on the arc axis.

Nevertheless many process determining factors such as the heat flux to the filler wire and the parent material or the current path and the resulting electromagnetic forces cannot be determined by experimental methods. Furthermore, a detailed process diagnostic is made more difficult by the material transfer.
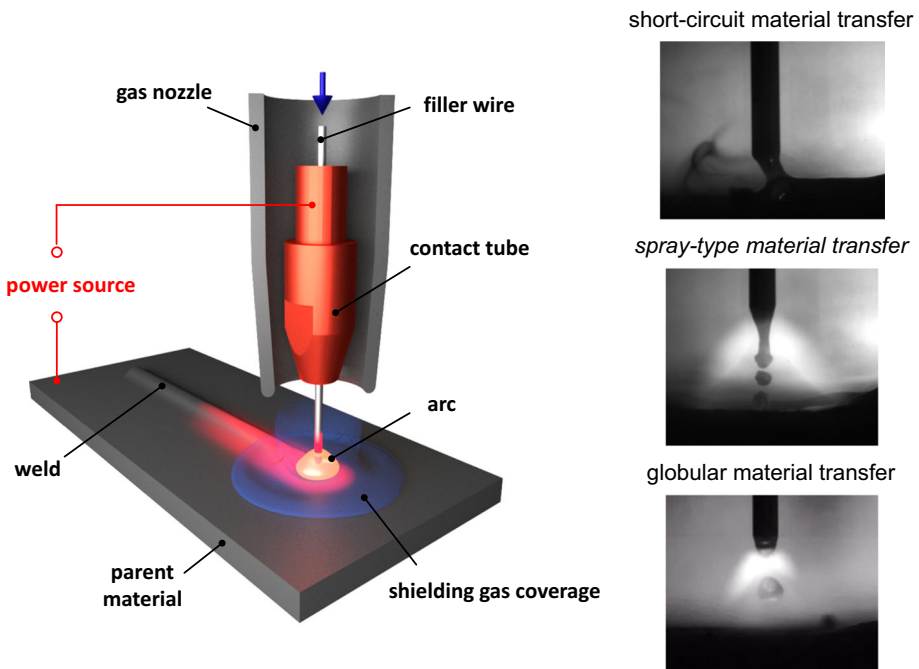
Fig. 1 Schematic illustration of the gas metal arc welding process (*left*) and common material transfer modes of gas metal arc welding (*right*)

Therefore, numerical methods are being used increasingly in order to quantify process variables and to improve process understanding. In earlier models of GMAW processes the influence of metal vapour was not considered [9–11]. This results in major differences between experimentally and numerically determined process variables, e.g. the temperature distribution in the arc or the filler wire and droplet shapes. Schnick et al. [12, 13] present a numerical investigation of a stationary GMAW arc in which they point out that the high radiative emission of iron vapour causes a minimum in the radial temperature distribution. In their treatment, Schnick et al. use an interface tracking technique with analytically defined and time-variant shapes for the filler wire and the parent material. The comparison of the numerically calculated temperature profiles in the arc via optical emission spectroscopy (OES) of Zielinska [5] shows a very good agreement. Furthermore it is pointed out, that the characteristics of the arc, e.g. the current path and the attachment of the arc at the filler wire dramatically change with increasing vaporization rates [13].

The metal evaporation is in turn determined by the heat flux profile at the filler wire surface. Numerous investigations dealing with the heat and charge transfer phenomena at anodic surfaces were presented by Pfender and Heberlein [14, 15]. Krivtsun et al. [16] present a complex model of the electric charge transfer in the anode region of an evaporating anode and couple it with a simplified arc model in which the changes of the electrode shapes are omitted as well [17].

More complex models of GMAW-processes [18–20] contain a self-consistent calculation of the vaporization rate of the filler wire on the basis of the local wire surface temperature and consider the influence of metal vapour on the thermophysical and radiation properties of the plasma. The change in the filler wire and droplet shapes are considered by using an interface capturing technique based on the volume of fluid (VOF) method by Hirt and Nichols [21]. In the recent past, the influence of different shielding gas compositions, e.g. a common gas mixture in technical application of 82% Argon and 18% carbon dioxide, on the process capability were analysed as well [22].

In addition to increasing the complexity of numerical models, the targeted combination of experimental and numerical methods is useful in order to analyse a wide range of different influencing variables in gas metal arc welding with an acceptable time effort and degree of complexity of the necessary numerical models.

In this article we summarize our analysis of the last years concerning the influence of metal vapour on gas metal arc welding processes of mild steel in spray as well as pulsed material transfer mode. In particular, the analysis of a large number of different shielding gas compositions on the example of a spray arc is intended to illustrate the extent to which already simplified models can be used with combination of experimental investigations concerning filler wire and metal vapour shapes in order to analyse complex cause-effect-chains with a high degree of accuracy. A detailed analysis of the influence of dynamic metal evaporation in GMAW pulsed arc welding using a VOF-model [19] is summarized in the second part of this paper.

Influence of Metal Vapour and Different Shielding Gas Components on a Spray Arc

In GMAW, metal vapours are primarily generated at the vaporizing filler wire. Due to the process gas flow, they are subsequently transported through the core of the arc and are therefore present in high concentration in the arc plasma. The process-determining

influence on the arc and thus the properties of the welding process both result from the evaporation processes on the filler wire and the high concentrations of metal vapour in the arc. The composition of the metal vapour is significantly determined by the composition of the filler wire. In the case of iron-based wires, due to their high iron concentration in the wire, the vapour mainly consists of iron vapour, which is considered in the most frequent investigations in the literature [2, 4–8, 12, 13, 18–20, 22] including this publication. However, other metal vapours such as copper, manganese, chromium and nickel are expected to exhibit similar behaviour patterns due to their increased radiation emissions [2] compared to the shielding gases used, such as argon, oxygen, nitrogen, helium, hydrogen or nitrogen.

The metal evaporation at the filler wire depends on many process parameters, including welding current, stickout length, wire and shielding gas composition as well as the material transfer type. Due to the explosion-like break-up of the metal bridge, short-circuit-proof processes cause considerably higher metal evaporation than short-circuit-free processes with the same electrical current. Furthermore, short-circuit-free pulsed arc processes with comparatively high arc currents in the pulse phase of approximately 400 A emit fewer emissions than short arc processes with significantly lower arc current of approximately 150 A [23].

In addition to the formation of a radial temperature minimum in the arc axis, the current flow in the arc and thus the speed and pressure distributions in the arc change significantly with increasing vaporization rates. Figure 2 shows this influence of iron vapour on a spray arc. The results shown in the figure were obtained by applying a simplified arc model in which the filler wire shape and temperature distribution in the filler wire were not calculated self-consistently but are derived using experimental observations. This approach will be discussed further in the text.

The calculations illustrate that the radiation emission is increased extremely even with small proportions of iron and leads to the formation of a radial temperature minimum in the arc axis because of the high radiation losses in the metal-vapour-dominated arc core. The sharp boundary of the iron core results from demixing processes in the plasma in which more easily ionisable particles (in this case, iron in comparison to argon) accumulate in regions with lower temperatures [3]. To a crucial extent, the current flow in the arc is altered by the high radiation losses in the arc core. The largest proportion of the current flows via the peripheral arc region dominated by argon since this exhibits a higher electric conductivity because of the higher plasma temperature [19].

The increased current flow in the edge regions of the arc results in a shift of the maximum of the flow velocity into the edge regions, caused by the increased Lorentz forces in that area. In the arc axis, the velocities are significantly lower compared to the edge area. At high evaporation rates, the current flow through the arc axis decreases further or even causes a backflow directed from the parent material to the filler wire, see Fig. 2, at the bottom left.

The pressure distribution at the electrodes is particularly interesting. The highest pressure is not obtained at the axis of the arc, as is the case, for example, for a TIG arc, but at the position at the circumference of the filler wire at which the evaporation begins. The resultant force effect in the case of a non-uniform evaporation over the circumference of the wire leads to a deflection of the molten filler wire (undoloid) which can be observed in high-speed images. In addition, there is a force effect on the underside of the filler wire, which is essentially determined by the arc attachment at the wire and leads to the deformation of the molten filler wire. The more concentrated the arc is on the filler wire, the greater the force effect at the filler wire tip and therefore the deformation.
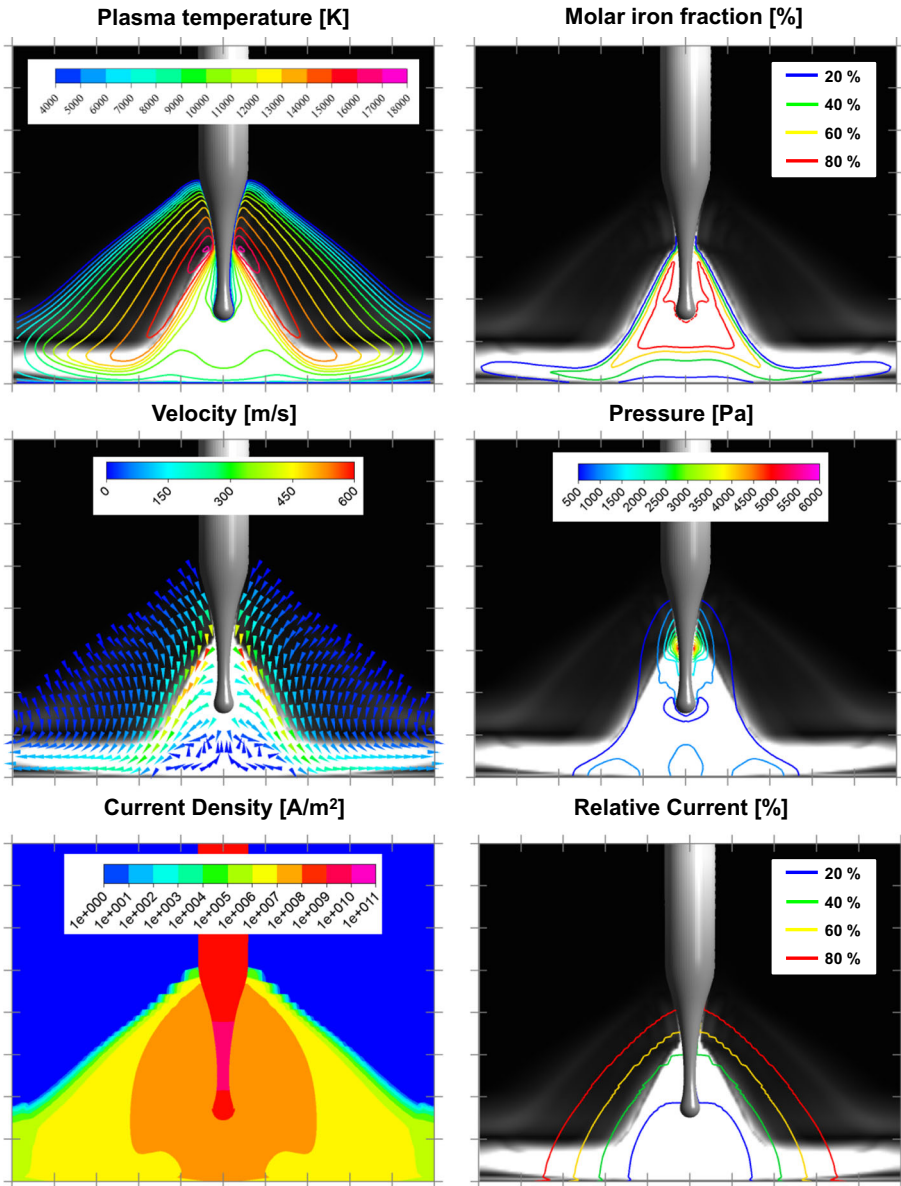
Fig. 2 Calculated distributions of plasma temperature (*top left*), molar iron fraction (*top right*), flow velocity (*middle left*), pressure (*middle right*), current density (*bottom left*) and relative current according to Eq. (1) (*background*: *grey shading* depending on the radiative emission) for a spray arc process (current: 350 A, wire feeding rate: 13 m/min, shielding gas: argon, filler wire: G3Si1, parent material: S235) [24]

Direct measurements of the evaporation rate of the filler wire are difficult, since welding fume measurements such as by Rose [23] can only capture the net welding fume emission of the process, in which a substantial part of the metal vapour is again absorbed by

condensation on the parent material and is thus not taken into account by the welding fume measurement.

For the simplified experimental determination of iron evaporation, the fact that a clear separation between the metal vapour core and the surrounding shielding gas results from the demixing processes in the arc can be exploited, see Fig. 2 top right. The resulting large differences in the net emission at the edge of the iron core results in significant differences in brightness. These differences in brightness can be recorded by high-speed cinematography in combination with spectrally selective filters and evaluated by subsequent contour detection.

In the case of an argon filter with a wavelength of 810 nm, the arc core, dominated by iron vapour, is dark and the differences in brightness can be evaluated by means of contour detection, see Fig. 3. By the use of a laser illumination the electrode shapes can be determined as well. Thus, the specific and temporally averaged electrode shapes can be comparatively easily converted into a numerical model by defining a fluid–solid interface and a corresponding unstructured mesh [12, 24]. In the calculations presented in Fig. 2 the extracted filler wire shapes using a spray arc process with a current of 350 A with a pure argon shielding gas (red lines in Fig. 5) has been used. In order to account for the deformation of the meld pool, the extracted profile has been shifted upwards in the direction of the contact tube.

Assuming a uniform temperature T_{max} below the point at the filler wire melt, where the evaporation begins and assuming a linear temperature decrease to the melting temperature at the point at the filler wire, where the deformation begins, an approximated filler wire temperature profile could be extracted from high speed images, Fig. 4. By iteratively adjusting the temperature T_{max} in order to match the observed metal vapour forms, it is also possible to make important statements about the evaporation rate of the filler wire, which are not possible by experimental investigations so far. In the calculations presented in Fig. 2 the temperature distribution in the filler wire shown in Fig. 4 has been used.

High speed imaging (10 kHz) with laser lightning (5 kHz) and argon filter (808±3 nm)
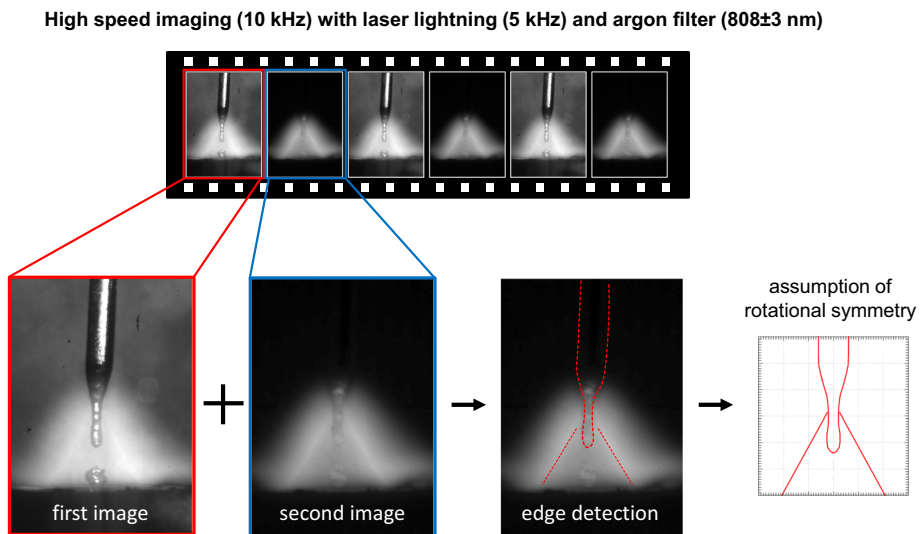
Fig. 3 Extraction of electrode and metal vapour core shapes from high speed images using laser lightning and spectral selective filters
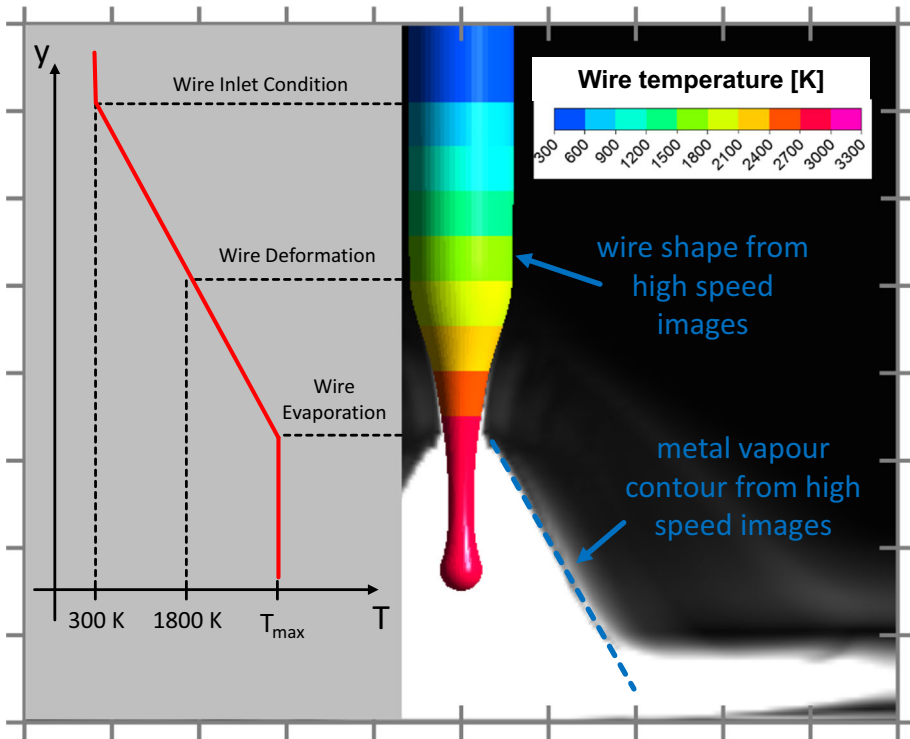
Fig. 4 Calculation of the filler wire temperature profile corresponding to high speed images of the wire contour and the metal vapour core

Through this combination of experimental and numerical methods, application-oriented process analyses, e.g. on the influence of different shielding gas compositions on the arc properties [24], can be carried out with a reasonable calculation and time effort. Figure 5 shows the influence of different shielding gases on the formation of the iron vapour core in a spray arc. The larger the metal evaporation on the filler wire, the wider the metal core will be. All investigated gas admixtures to argon lead to an increase in the metal evaporation from the filler wire. Compared to oxygen, the same admixture of carbon dioxide causes a greater increase in metal evaporation. Hydrogen causes the greatest increase in metal evaporation for equal mixing ratios. The increase in metal evaporation also suggests an increase in welding fume emissions from the process. The increase in the evaporation rate correlates with an increased heat flux at the filler wire surface caused by higher thermal conductivities of the shielding gas mixtures compared to pure argon. Especially the thermal conductivity in the range of the surface temperature of nearly 3000 K is of interest for the heat conduction into the filler wire, Fig. 5 in [24]. In this range, shielding gases with hydrogen admixtures of 5% to argon have thermal conductivities which are nearly seven times higher, admixtures of 70% helium to argon have five times higher and admixtures of 18% carbon dioxide to argon have two times higher thermal conductivities than pure argon.

While admixtures of helium and hydrogen have only a small influence on the average form of the unduloides, the average length of the latter changes considerably as a result of the admixture of carbon dioxide and oxygen. For admixtures higher than 2.5% carbon
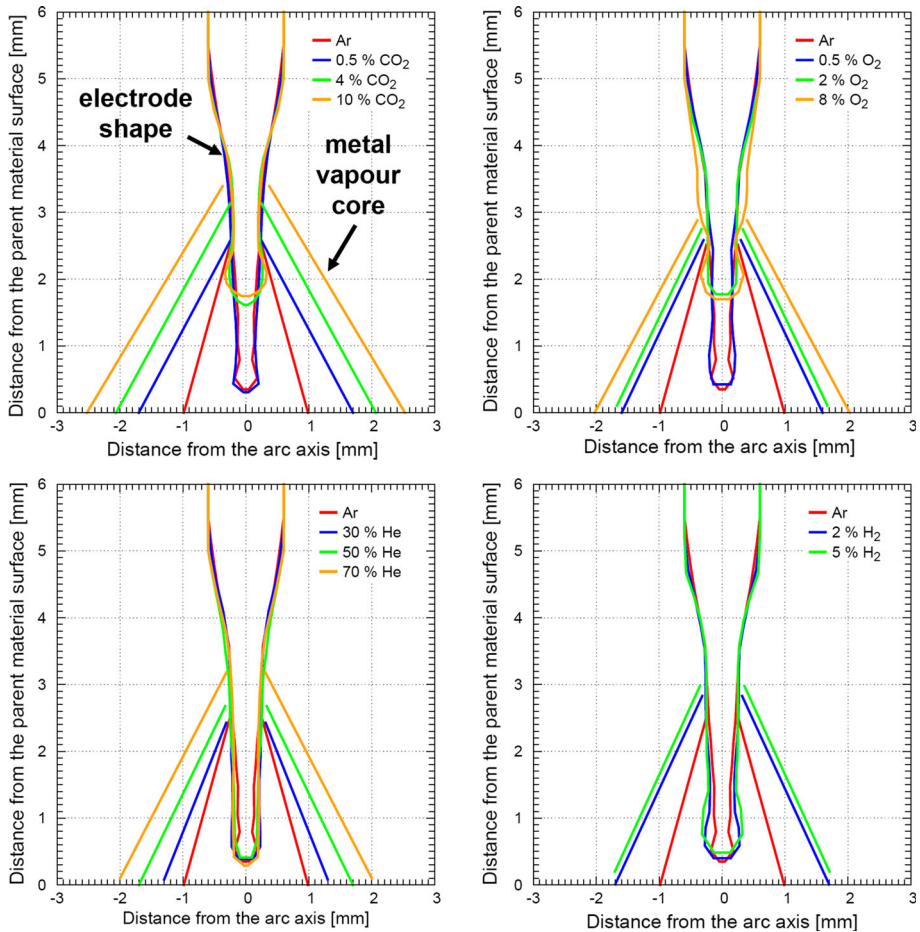
Fig. 5 Time averaged shapes of the filler wire and metal vapour cores for a spray arc process with different shielding gas admixtures of carbon dioxide, oxygen, helium or hydrogen gained from experimental observations [24]

dioxide or 1.5% oxygen, a clear shortening of the unduloid can be observed. For admixtures higher than 4% carbon dioxide or 4% oxygen, no further shortening of the mean unduloide length can be observed.

Using such a numerical arc model [24] it was found that in most cases iron vapour in the arc exerts a greater influence on the arc properties than the thermophysical properties of the shielding gas components itself. The radiation-induced cooling of the metal vapour core leads to a significant reduction in the electrical conductivity compared to the edge regions and thus to a widening of the current path. The increased evaporation leads to an expansion of the arc, to a displacement of the arc attachment in the direction of the contact nozzle and to a defocusing of the arc attachment at the parent material.

A further change of the process behaviour with regard to the type of material transfer can be observed with higher admixtures of carbon dioxide. While the material transfer takes place in a symmetrical manner with respect to the axis of the filler wire during all the admixtures of oxygen, helium and hydrogen, or when less than 10% carbon dioxide is

admixed, the droplet detachment becomes increasingly unsymmetrical when more than 10% carbon dioxide is admixed to the shielding gas, see Fig. 6. As a result, the entry range of the droplets into the weld pool and thus the heat input into the weld pool changes significantly.

This contrary influence of carbon dioxide admixtures over 10% compared to all other discussed admixtures of oxygen, helium or hydrogen results from an increased pressure force at the tip of the filler wire caused by a increased arc constriction, see Fig. 7. Especially the high volumetric enthalpy of the resulting shielding gas leads to this arc constriction. Besides the increased pressure forces at the tip of the filler wire, the arc constriction determines an increased current density in the filler wire tip and therefore an increased Lorentz force. The high pressure at the filler wire tip as well as the increased Lorentz forces in the wire tip leads to the unsymmetrical material transfer, see Fig. 6.

## Influence of Dynamic Metal Evaporation in GMAW Pulsed Arc Welding

In pulsed gas metal arc welding, the wire and droplet formation is essentially determined by the arc attachment at the filler wire. The arc attachment in turn is influenced by the metal evaporation from the filler wire, which is highly dynamic in the pulse phase due to the variable heating of the filler wire. The analysis of these dynamic processes can be carried out by the use of numerical models. Both the variable wire and droplet shapes as well as the changes in the arc properties have to be taken into account as a function of the metal evaporation in the model. Experimental investigations with regard to wire and droplet formation as well as the temperature distribution at the metal surfaces and the distribution of temperature and metal vapour in the arc can be used to validate these numerical models.

In the following, the influence of the dynamic metal evaporation is described for a pulsed gas metal arc welding process with the parameters shown in Table 1.

The current run and the wire and droplet formation observed by high-speed images [23] are shown in Fig. 8.
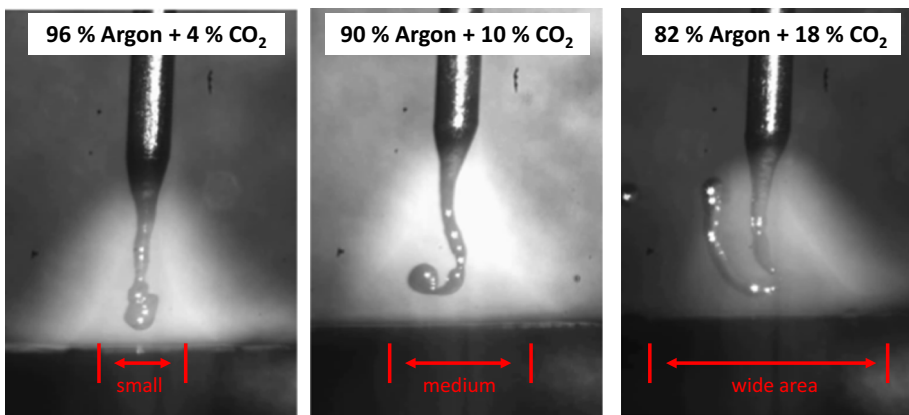

Fig. 6 Changing material transfer and entry area for a spray arc process with different shielding gas admixtures of carbon dioxide to argon [24]
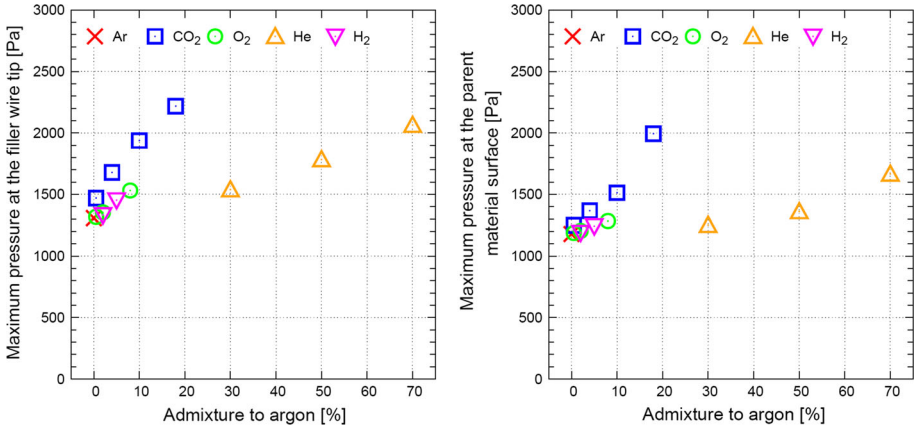
Fig. 7 Calculated maximum pressure at the wire tip (*left*) and on the parent material surface (*right*) for a spray arc process with different shielding gas admixtures of carbon dioxide, oxygen, helium or hydrogen [24]

Table 1 Parameters of the investigated pulsed GMAW process

| Parameter	Value
Pulse time	10 ms
Pulse current I ground current I mean current	420 A I 50 A I 125 A
Wire diameter	1.2 mm
Shielding gas	Argon
Filler wire material I parent material	G3Si1 I S235 JG2
Wire feeding speed I welding speed	4 m/min I 0.3 m/min
Distance contact tip—parent material	15 mm
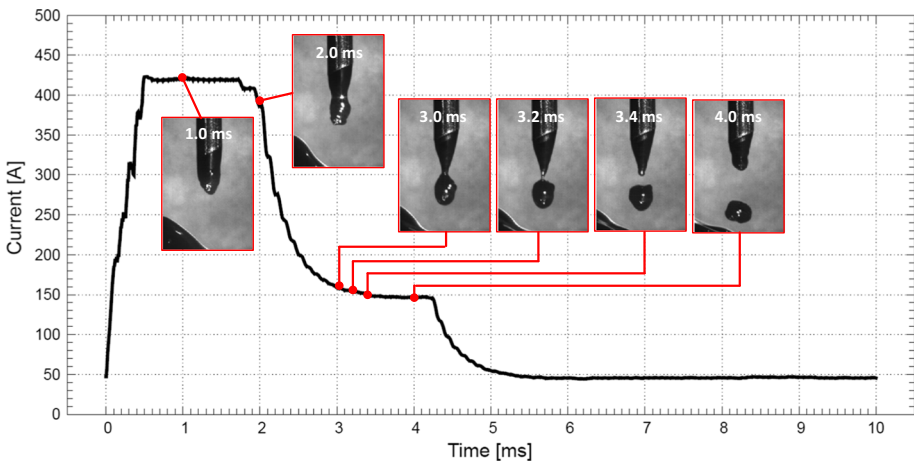
Fig. 8 Current run and high speed images of a pulse process with the parameter shown in Table 1

Using a self-consistent calculation of the iron evaporation based on the time-varying plasma and metal temperatures and the calculation of the variable filler wire and droplet shapes it is possible to calculate this complex interaction between the arc and the material transfer with a numerical model [19, 20]. In the model used, temperature dependent properties of mild steel [19] and argon-iron-plasmas [2] are used. The comparison with spectroscopic measurements shows a very good agreement with regard to the temperature and iron distribution in the arc [25]. Furthermore, the model gives very good correlations with respect to the calculated wire and droplet shapes determined by high speed images [23].

Figure 9 shows the distributions of the plasma temperature and the iron concentration, calculated using the model described in [19, 25], for different time points within the current run. For the description of the variable current path in the filler wire and the arc, the integral current is calculated according to Eq. 1.

$$I_{rel} = -\frac{2\pi \int_0^R j_y x \, dx}{I(t)} \tag{1}$$

In Eq. (1) j_y is the axial electrical current density, x is the radial coordinate and $I(t)$ is the total current for the time t within the current run. Figure 10 shows the distribution of this integral current, based on the instantaneous value of the pulse current. At the end of the background current phase, the amount of iron in the arc is minimal, and the arc is focussed
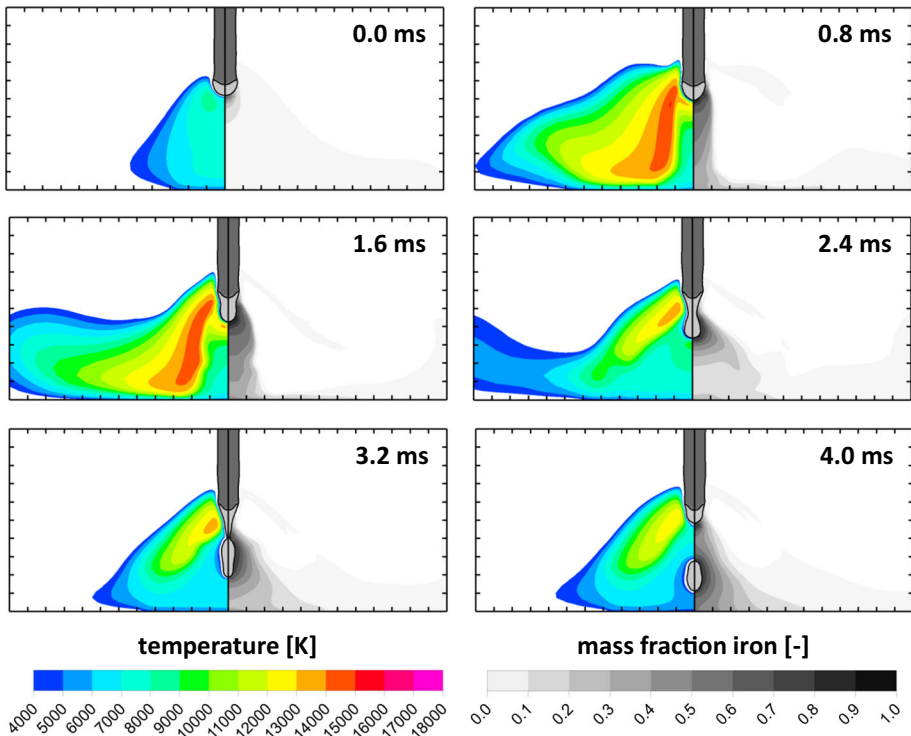
Fig. 9 Calculated temperature und mass fraction of iron of a pulse process with the parameter shown in Table 1 for various times within the current run
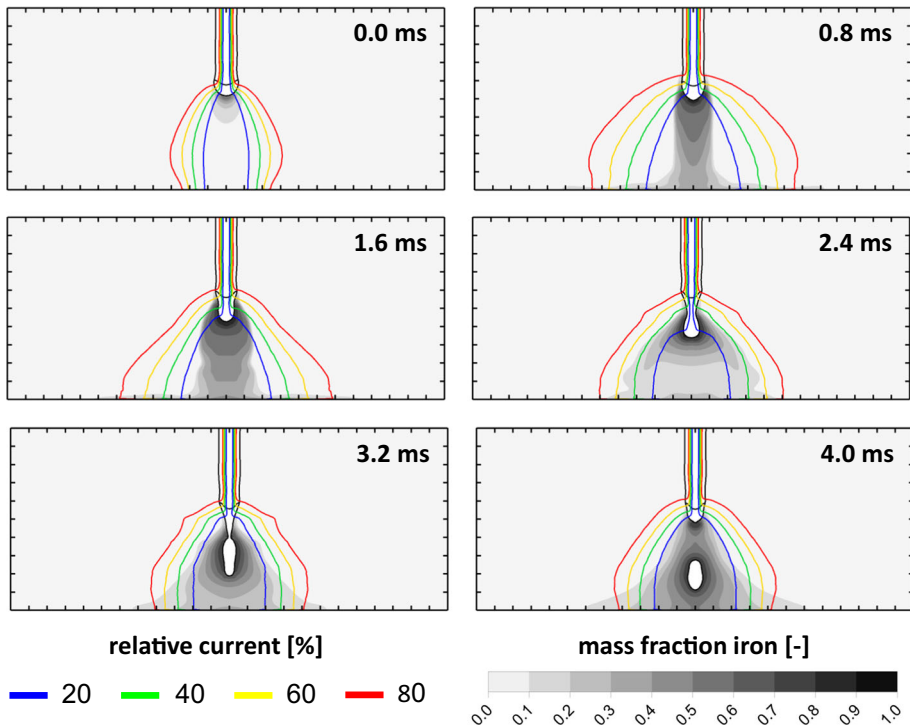
Fig. 10 Calculated current path and mass fraction of iron of a pulse process with the parameter shown in Table 1 for various times within the current run

at the wire tip. At the beginning of the current rise, the iron evaporation on the filler wire increases rapidly, while the iron is transported with the flow through the centre of the arc. Already within the current rise slope, the mass fraction of the iron core is on average more than 30%. As a result of the high radiation of the iron, a minimum is formed in the radial temperature distribution. The temperatures in the arc core reach values between 8000 and 10,000 K and up to 16,000 K at the arc edges.

Within the high current phase, the evaporation rate of the filler wire and thus the diameter of the iron core increases further. The cause of the drastic increase in iron evaporation is the heating of the wire surface due to the absorption of electrons. The heat flow into the filler wire resulting from the electron absorption follows the current profile proportionally and is approximately eight times greater in the high current phase than in the ground current phase. During the high current phase, the heat input caused by the electron absorption is constant, while the resistive heating increases see Fig. 11 left. This circumstance is caused by both the constriction that occurs and by the heating of the filler wire and the resulting reduction in the electrical conductivity. It can be visualized by the balancing of the voltage drop within the filler wire, see Fig. 11 right.

As a result of the increased iron evaporation on the filler wire, the arc attachment is shifted towards the contact tip. The reason for the change in the arc attachment is the mixing of the evaporated iron with the plasma, which leads to a reduction of the plasma temperature and thus to a reduction of the electrical conductivity at the surface of the filler wire. This effect is supported by the absorption of the radiation above the arc attachment,
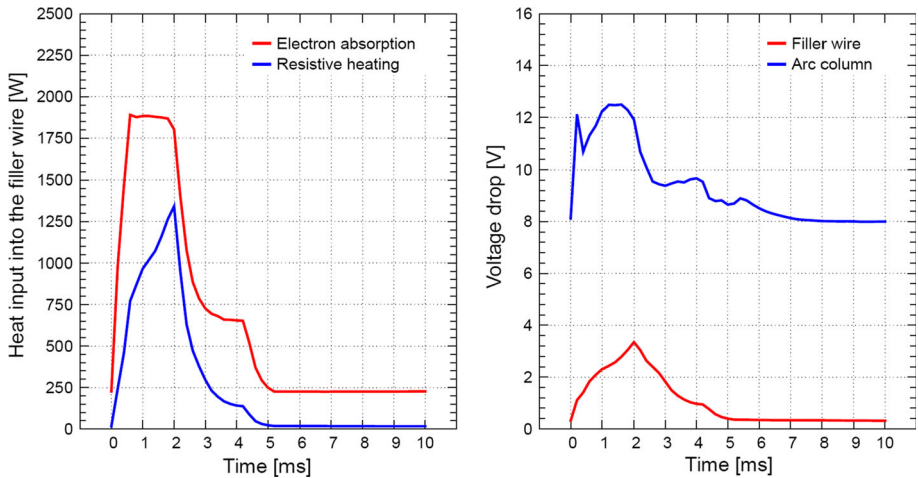
Fig. 11 Calculated heat flow through electron absorption at the wire surface and resistive heating (*left*) as well as voltage drop in the filler wire and arc column (*right*) of a pulse process with the parameter shown in Table 1

which has a very high intensity, especially in the high current phase due to the high radiation emission of the arc core [25].

Particularly interesting is the fact that at the time of the filler wire constriction (2.4 ms) only about 40% of the current is transported through the constriction. As a result, the current flow which is responsible for the constricting pinch force is significantly lower than the total current at that time. Shortly before detaching the droplet (3.2 ms), less than 10% of the total current is transported through the molten metal bridge between the wire and the droplet. Due to the reduced current flow and the resultant reduced effect of the lorentz force on the molten metal bridge, nearly spatter-free droplet detachment is observed in pulse arc welding. After the droplet detachment, over 80% of the total current is transported through the edge regions of the arc, in which the mass fraction of iron is below 10%. The plasma temperatures are around 8 000 K in the core of the arc and reach up to 13 000 K at the arc edges.

The calculations show that the pulsed arc is characterized by a high dynamic, which results on the one hand from the current run and the droplet detachment, but to a considerable extent on the other hand from the variable arc attachment at the filler wire. The displacement of the arc in the direction of the contact nozzle is essentially caused by the beginning iron evaporation on the filler wire, which results largely from the heating of the electrons absorbed at the wire surface. The resistance heating within the filler wire is a decisive factor in the heating of the filler wire. Further components in the energy balance, such as the heat conduction from the arc or the cooling due to the evaporation, are of secondary importance, see Table 2.

The sensitive influence of metal evaporation on wire and droplet formation can be illustrated by limiting the metal temperature to a maximum value T_{max} within the calculation of the metal vaporization mass flux $\hat{m}_{VAP}$ corresponding to Eq. (2) and the vapour pressure p_{VAP} according to Eq. (3) [19]. By setting lower maximum temperatures, the metal evaporation is consequently reduced as well.

Table 2 Balance of the calculated and time averaged heat flow in the filler wire for the pulse and ground current phases of the pulse process with the parameter shown in Table 1

Heat flow	High current phase (0.6–2 ms) (W)	Ground current phase (5–10 ms) (W)
Electron absorption	1890	225
Resistive heating	1200	20
Heat conduction into the filler wire	150	30
Heat radiation into the filler wire	50	15
Vaporization cooling	−100	−30

$$\widehat{m}_{VAP} = \sqrt{\frac{M_B}{2\pi R}} \left(\frac{p_{VAP}}{\sqrt{\min(T_M, \mathbf{T_{max}})}} - \frac{X_{G,B}p}{\sqrt{T_G}} \right) \tag{2}$$

In Eq. (2) M_B is the molar mass of the metal vapour component, R is the ideal gas constant, p_{VAP} is the vapour pressure, $X_{G,B}$ is the molar fraction of the metal vapour component in the gaseous phase, p is the pressure in the gaseous phase and T_M and T_G are the temperatures of the metal and gaseous phase respectively.

$$p_{VAP} = p \exp \frac{-H_{VAP}M_B}{R} \left(\frac{1}{\min(T_M, \mathbf{T_{max}})} - \frac{1}{T_{m,B}} \right) \tag{3}$$

In Eq. (3) H_{VAP} is the heat of vaporization and $T_{m,B}$ is the boiling temperature of the filler wire material.

Figure 13 shows the calculated distribution of the plasma and droplet temperatures as well as the iron vapour distribution in the arc and its effect on wire and droplet formation. The calculated values are shown for different maximum temperatures of 2950 K, 3000 K and 3050 K within the calculation of the evaporation rate. Due to the exponential dependence of the evaporation on the metal temperature, even slight temperature changes of 100 K have a dominant effect on the arc attachment and the droplet detachment. In the presented calculations, a maximum temperature of 2950 K corresponds to a maximal vaporization rate of 3.79 mg/s, 3000 K to 4.84 mg/s and 3050 K to 9.45 mg/s respectively.

At low evaporation rates ($T_{max} = 2950$ K) the arc attachment is more concentrated at the wire tip, the molten area at the filler wire is significantly longer and the material transfer is finer. At higher evaporation rates ($T_{max} = 3000$ K), the material transfer is significantly coarser due to the more defocused arc. At a high evaporation rate ($T_{max} = 3050$ K), no droplet detachment occurs within the current run due to the defocused arc. The metal vapour influence could be illustrated by the current density as well, see Fig. 12.

Observations on pulsed arc processes show that with increased metal evaporation, the droplet detachment no longer occurs regularly within each pulse, but droplet growth takes place over several pulse phases. The results show that the metal evaporation has not only a significant influence on the arc properties, but also on wire and droplet formation (Fig. 13).
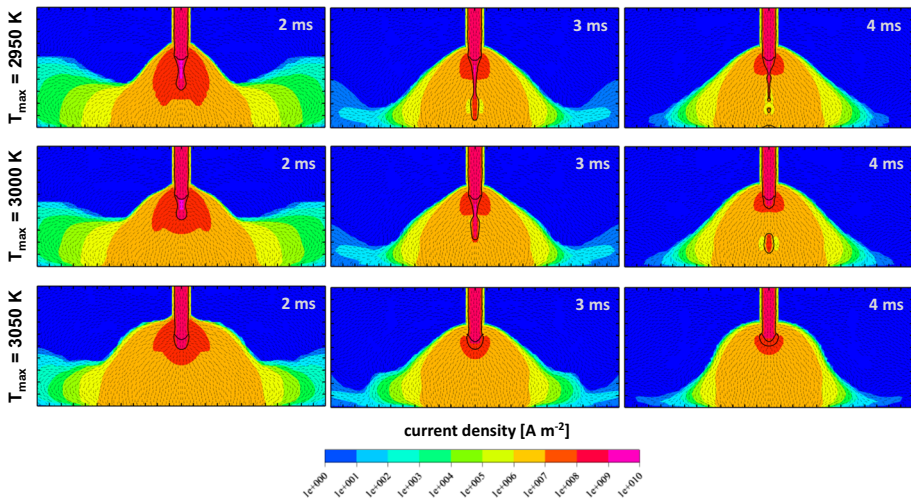
Fig. 12 Calculated current density distribution of a pulse process with the parameter shown in Table 1 for various times within the current run and different maximum temperatures

Conclusions

In this article we summarize our analysis of the last years concerning the influence of metal vapour on gas metal arc welding processes of mild steel in spray as well as pulsed mode. In order to analyse the influence of a large number of different shielding gas compositions, a targeted combination of numerical and experimental methods could be useful to analyse the complex cause-effect-chains with a high degree of accuracy as well as a low computational effort. As a result, the statements can not only be used for basic research, but also for welding processes in technical application, in which pure argon is only rarely used as a shielding gas.

Concerning the influence of different shielding gas components in a spray arc it could be shown, that the resulting change of the vaporization rate at the filler wire and the higher concentration of metal vapour in the arc region often has a greater influence on the arc properties than the thermophysical properties of the shielding gas mixture itself. In summary, it may be stated that the effects of shielding gas components on the gas metal arc welding process cannot be deduced only from the thermophysical properties of the gas components but it is instead necessary to take into account the indirect influences on the metal vaporisation and the resulting metal transfer.

Concerning the pulsed gas metal arc welding process it could be shown, that the changing vaporization rate of the filler wire within the current run, mainly determined by the electron absorption, has a great influence not only on the arc properties but also on the arc attachment. With increasing vaporization rates of the filler wire, the arc attachment is shifted upwards to the contact tip. At the time of droplet detachment less than 10% of the instantaneous current is transported through the constriction area. As a result, the pinch effect has a much smaller influence on the droplet detachment of gas metal arc welding processes of mild steel in pure argon shielding gas than is often assumed in the literature. In the case of high vaporization rates of the filler wire, droplet detachment does not take place in every pulse cycle.
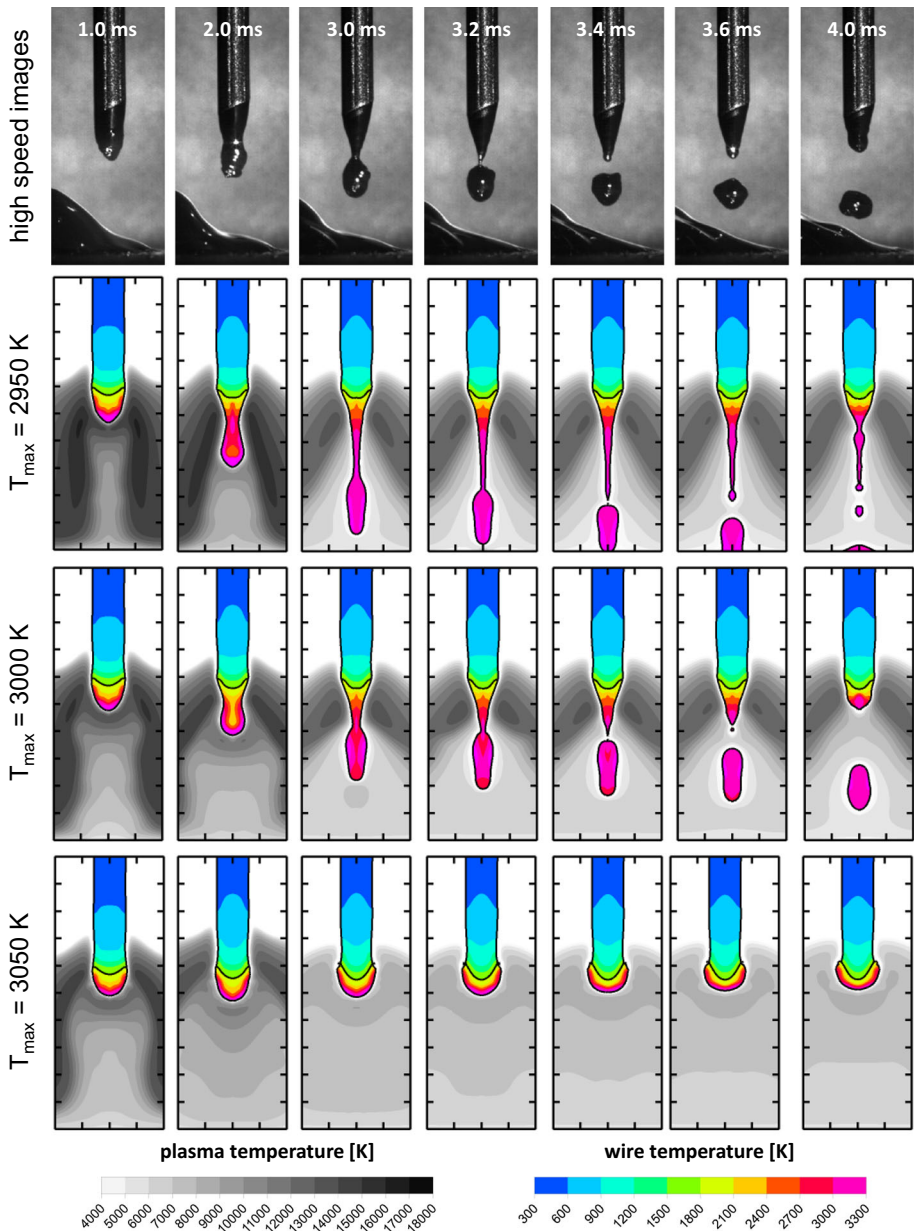
Fig. 13 Calculated shapes and temperature distributions in the filler wire and the droplet of a pulse process with the parameter shown in Table 1 for various times within the current run and different maximum temperatures in comparison to high-speed images of [22]

The high sensitivity of the iron evaporation illustrates how important a detailed knowledge of the heat and charge transfer in the anode layer is in order to understand the process behaviour of GMAW.

References

1. Norish J (2006) Advanced welding processes. Woodhead Publishing. https://www.elsevier.com/books/advanced-welding-processes/norrish/978-1-84569-130-1
2. Murphy AB (2010) The effects of metal vapour in arc welding. J Phys D Appl Phys 43:434001
3. Murphy AB (2016) A perspective on arc welding research: the importance of the arc, unresolved questions and future directions. Plasma Chem Plasma Process 35(3):471–489
4. Goecke SF (2004) Auswirkungen von Aktivgaszumischungen im vpm-Bereich zu Argon auf das MIG-Impulsschweissen von Aluminium. Dissertation TU Berlin
5. Zielinska S, Musiol K, Dzierzega K, Pellerin S, Valensi F, de Izarra Ch, Briand F (2007) Investigations of GMAW plasma by optical emission spectroscopy. Plasma Sources Sci Technol 16:832
6. Rouffet ME, Wendt M, Goett G, Kozakov R, Schöpp H, Weltmann KD, Uhrlandt D (2010) Spectroscopic investigation of the high-current phase of a pulsed GMAW process. J Phys D Appl Phys 43:434003
7. Tsujimura Y and Tanaka M (2013) Plasma diagnostics in gas–metal arcs during welding. In: IIW conference Denver 2012, SG 212-meeting, IIW Doc. 212-1237-12
8. Kozakov R, Gött G, Schöpp H, Uhrlandt D, Schnick M, Hässler M, Füssel U, Rose S (2013) Spatial structure of the arc in the pulsed GMAW process. J Phys D Appl Phys 46:224001
9. Haidar J, Lowke JJ (1996) Predictions of metal droplet formation in arc welding. J Phys D Appl Phys 29(12):2951
10. Fan HG, Kovacevic R (2004) A unified model of transport phenomena in gas–metal arc welding including electrode, arc plasma and molten pool. J Phys D Appl Phys 37:2531
11. Xu G, Hu J, Tsai HL (2009) Three-dimensional modeling of arc plasma and metal transfer in gas metal arc welding. Int J Heat Mass Transf 52:1709–1724
12. Schnick M, Füssel U, Hertel M, Spille-Kohoff A, Murphy AB (2010) Metal vapour causes a central minimum in arc temperature in gas–metal arc welding through increased radiative emission. J Phys D Appl Phys 43:022001
13. Schnick M, Füssel U, Hertel M, Haessler M, Spille-Kohoff A, Murphy AB (2010) Modelling of gas–metal arc welding taking into account metal vapour. J Phys D Appl Phys 43:434008
14. Pfender E (1980) Energy transport in thermal Plasmas. Pure Appl Chem 52:1773–1800
15. Heberlein J, Mentel J, Pfender E (2010) The anode region of electric arcs: a survey. J Phys D Appl Phys 43(2):023001
16. Krivtsun I, Demchenko V, Lesnoi A, Krikent I, Poritsky P, Mokrov O, Reisgen U, Zabirov A, Pavlyk V (2010) Modelling of electromagnetic processes in system'welding arc—evaporating anode': I. Model of anode region. Sci Technol Weld Join 15:457–462
17. Krivtsun I, Demchenko V, Lesnoi A, Krikent I, Poritsky P, Mokrov O, Reisgen U, Zabirov A, Pavlyk V (2010) Modelling of electromagnetic processes in system 'welding arc—evaporating anode': II. Model of arc column and anode metal Sci. Technol Weld Join 15:463–467
18. Boselli M, Colombo V, Ghedini E, Gherardi M, Sanibondi P (2012) Two-dimensional time-dependent modelling of fume formation in a pulsed gas metal arc welding process. J Phys D Appl Phys 46:224006
19. Hertel M, Spille-Kohoff A, Füssel U, Schnick M (2013) Numerical simulation of droplet detachment in pulsed gas–metal arc welding including the influence of metal vapour. J Phys D Appl Phys 46:224003
20. Ogino Y, Hirata Y (2015) Numerical simulation of metal transfer in argon gas-shielded GMAW. Weld World 59(4):465–473
21. Hirt CW, Nichols BD (1981) Volume of fluid (VOF) method for the dynamics of free boundaries. J Comput Phys 39:201–225
22. Ogino Y, Yoshinori Hirata, Murphy AB (2016) Numerical simulation of GMAW process using Ar and an Ar-CO2 gas mixture. Weld World 60(2):345–353
23. Rose S (2013) Einfluss des Werkstoffübergangs auf das dynamische Prozessverhalten beim Metall-schutz-gasschweißen. Dissertation TU Dresden
24. Hertel M, Niese J, Rose S, Häßler M, Füssel U, Uhrlandt D (2015) Experimental und numerical investigations into the influence of the shielding gas composition on the GMA spray arc process. Weld Cut 14(5):234–441
25. Hertel M, Rose S, Füllel U (2016) Numerical simulation of arc and droplet transfer in pulsed GMAW of mild steel in argon. Weld World 60(5):1055–1061